Electronic Supplementary Information

Synthetic Manganese-Calcium Oxides Mimic the Water-Oxidizing Complex of Photosynthesis Functionally and Structurally

Ivelina Zaharieva,*[a] M. Mahdi Najafpour,[b,c] Mathias Wiechen,[b] Michael Haumann,[a] Philipp Kurz*[b] and Holger Dau*[a]

[a] *Fachbereich Physik, Freie Universität Berlin, Arnimallee 14, 14195 Berlin, Germany.*

E-mail: ivelina.zaharieva@fu-berlin.de; holger.dau@fu-berlin.de;

Fax: +49 30 838 56299; Tel: +49 30 838 53581

[b] *Institut für Anorganische Chemie, Christian-Albrechts-Universität zu Kiel, 24118 Kiel, Germany. E-mail: phkurz@ac.uni-kiel.de; Fax: +49 431 880 1520; Tel: +49 431 880 5803*

[c] *Institute for Advanced Studies in Basic Sciences (IASBS), P. O. Box 45195-1159, 45195 Zanjan, Iran*

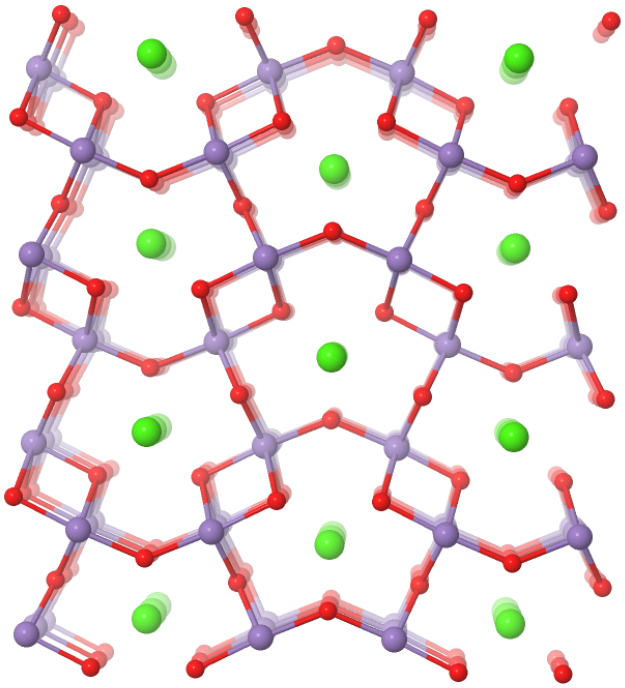

Figure S1. Solid state structure of the mineral marokite[1] from which different models of the manganese OEC can be cut out. Oxygen atoms are shown in red, Ca - green, and Mn - purple.

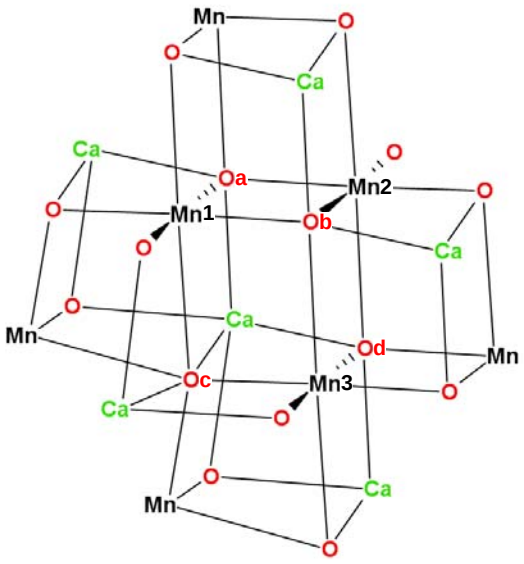

Figure S2. Structure of the mineral marokite ($CaMn_2O_4$) showing the saturated nature of the oxygen ligands in the bridging positions between metal ions (oxido bridges), which are of a μ_5-oxido (Oa, Ob and Od) or a μ_6-oxido (Oc) bridging type. The Mn-Mn distances found in marokite are clearly longer than the Mn-Mn distances of ~ 2.7 Å for di-μ-oxido bridged Mn ions in PSII. Mn-Mn distances in marokite: Mn1-Mn2, 2.91 Å; Mn1-Mn3, 3.16 Å; Mn2-Mn3, 3.19 Å; Mn1-Mn, 3.06 Å.

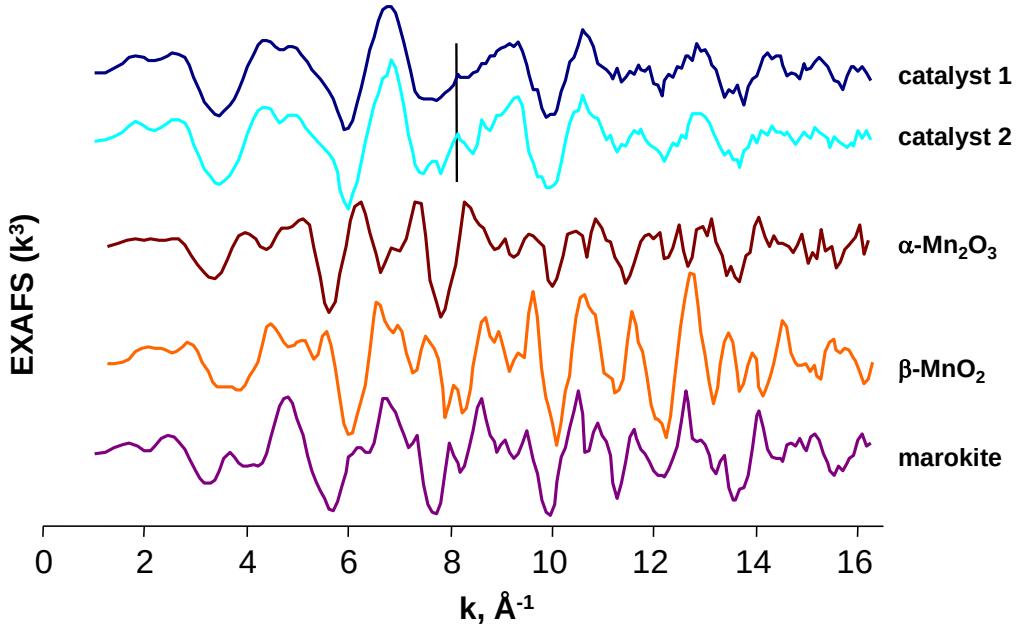

Figure S3. EXAFS spectra of catalysts **1** and **2**, and further Mn oxides recorded at the *K*-edge of manganese. The spectra of **1** and **2** are highly similar and show a peak that is characteristic for layered MnO_2 structures (at 8 $Å^{-1}$, indicated by a vertical line). The size of the peak indicates the extent of order in the MnO_2 layers;[2-6] in **1** and **2** its intensity is relatively low. The spectra of **1** and **2** are very different from the spectra of non-layered Mn oxides like β-MnO_2, α-Mn_2O_3 and marokite. β-MnO_2 has a structure where single chains of edge-sharing $Mn^{IV}O_6$ octahedra share corners with neighboring chains to form a framework containing tunnels with square cross sections that are one octahedron by one octahedron.[7] The structure of α-Mn_2O_3 is composed of densely packed edge- and corner-sharing $Mn^{III}O_6$-octahedra.[8] The structure of marokite is presented in Figures S1 and S2.

EXAFS simulations

The extracted spectrum was weighted by k^3 and simulated (least-squares fit) in k-space using all data points between 3 and 16 $Å^{-1}$ (20-1000 eV above the respective E_0). All EXAFS simulations were performed using the in-house software SimX3, after calculation of phase functions with the FEFF program (version 8.4, self-consistent field option activated).[9, 10] Atomic coordinates of the FEFF input files were generated on basis of the structure models shown in Figure 4. An amplitude reduction factor S_0^2 of 0.7 was found to reproduce the known coordination number of 6 for δ-MnO_2 and thus also was used in the simulation of the EXAFS spectra of the other compounds. For the Ca spectra, the amplitude reduction factor was 0.83 to match a coordination number of 8 in marokite; it was kept at this value for all Ca spectra. For simulation of the EXAFS oscillations leading to peaks labeled with an asterisk (*) in Figure S7, multiple scattering contributions were considered. Phase functions for the 2-leg (single-scattering), 3-leg and 4-leg paths were calculated by the FEFF program and used in the EXAFS fit.

The EXAFS simulation was optimized by a minimization of the error sum obtained by summation of the squared deviations between measured and simulated values (least-squares fit). To quantify the error, we also used the EXAFS R-factor, which increases linearly with the deviation between experimental and simulated data (International XAFS Society, Standards and Criteria Committee: Error Reporting Recommendations; http://www.i-x-s.org/). To determine the R-factor specifically with respect to the EXAFS oscillations corresponding to a distinct range of absorber-backscatter distances, we used the Fourier-filtered R-factor (R_F) described elsewhere.[11] The R-space used to estimate the error range of fit parameters was (1.1-6.0 Å) for the Mn spectra and (1.8-6.0 Å) for the Ca spectra. The error ranges of the fit parameters were estimated from the covariance matrix of the fit. The fit was performed using the Levenberg-Marquardt method with numerical derivatives.[11] Error ranges correspond to 68% confidence intervals of the corresponding fit parameters.

Correlation analysis of the fit results for the common Mn-Ca distance at about 3.1 Å. The proposed structural models predict the formation of Mn_3Ca cubanes with a common Mn-Ca distance of ~3.1 Å. In such cubanes, the expected coordination numbers are 3 for Ca-Mn interactions (each Ca "sees" 3 Mn atoms at this distance) and 1 for Mn-Ca distances (each Mn sees about 1 Ca). In our experimental data however, the coordination numbers are 0.4 for Ca-Mn and 2.4 for Mn-Ca interactions. This suggests that there may be also Mn-Mn vectors of about 3.1 Å length, possibly related to formation of Mn_4O_4 cubanes. The next three figures show the analysis of the question to what extent Mn^{III} and Ca ions contribute to this distance.

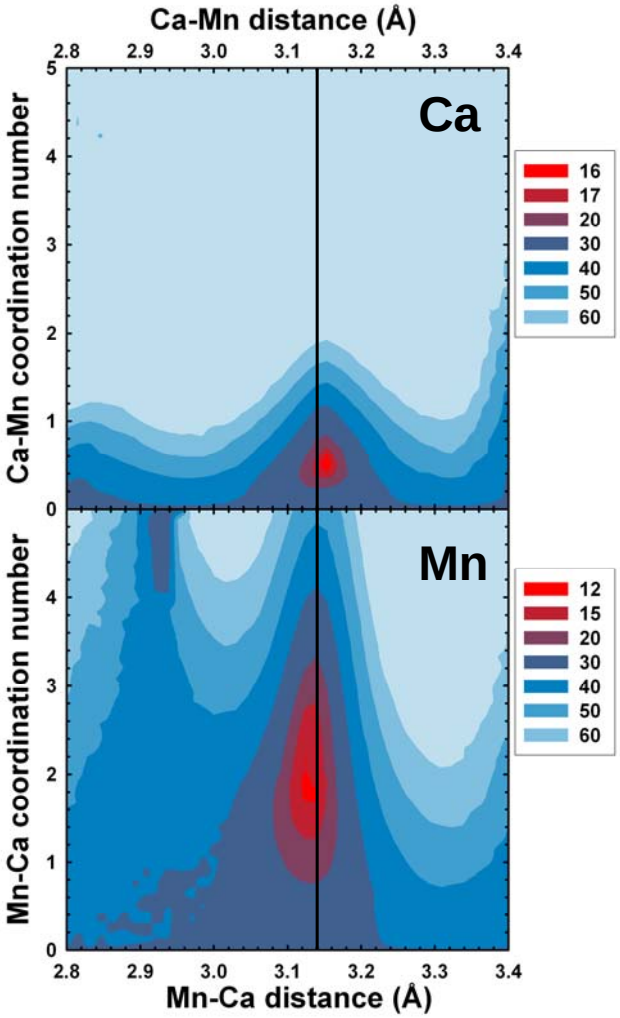

Figure S4. Contour plots for R_F-factor variations for simulations of EXAFS spectra obtained for catalyst **1** at the Ca and Mn edges, respectively. Variations of the Mn-Ca distances and the EXAFS coordination numbers are shown. The color code is such that red regions correspond to better fits and light blue areas correspond to inferior fits. A common Mn–Ca distance can be found at around 3.14 Å, possibly the distance between Ca and Mn in Mn_3Ca cubanes. The Mn–Ca distance in the Mn spectrum is slightly shorter than the one found in the Ca spectrum, which could be an indication that the corresponding interaction is not only a Mn^{IV}–Ca but probably also partly a Mn^{IV}–Mn^{III} distance. The latter is shorter and of course not visible in the Ca edge data. The plots were composed from 1600 individual fits. The range for the calculation of the R_F-factor was 2 – 4 Å. The number of shells was as shown in Table 1. All the parameters which are not fixed in Table 1 varied freely.

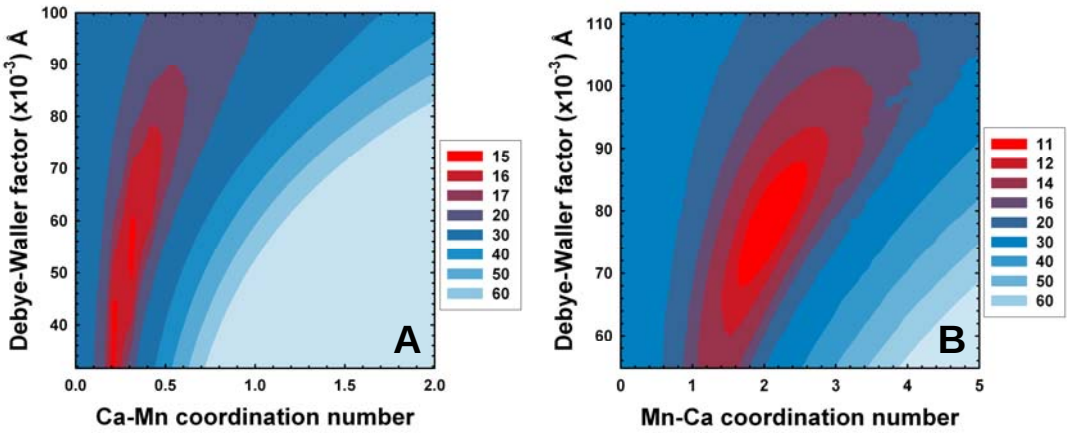

Figure S5. Error plots for simulations of EXAFS spectra obtained for **1** at the Ca and Mn edges with variations of metal-metal coordination numbers and Debye-Waller factors. These variations were carried out to test the hypothesis of a superposition of two distances at around 3.14 Å in the Mn spectrum (Mn^{IV}–Ca and Mn^{IV}–Mn^{III}). In the Ca spectrum (**A**), two very narrow minima are observed. Only one (at a coordination number of 0.35) is found at a physically meaningful value for the Debye-Waller factor (σ, elsewhere also denoted as Debye-Waller parameter). As expected, the minimum is much broader in the Mn spectrum (**B**) than in the Ca spectrum (two shells contribute simultaneously). The plots were composed from 1800 individual fits with shells as given in Table 1. The range for the calculation of the R_F-factor was 2 – 4 Å. The Mn–Ca distance was fixed to 3.14 Å for the simulation of both spectra.

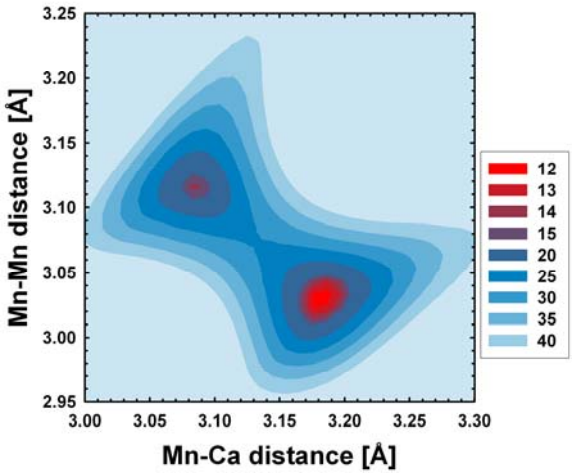

Figure S6. Contour plot of the R_F-factor visualizing the most likely Mn^{IV}–Ca and Mn^{IV}–Mn^{III} distances. The 3.11 Å distance in the Mn spectrum of oxide **1** was fitted with two shells (instead of only one): one Mn and one Ca shell. The analysis supports the presence of $Mn^{IV}_{2/3}$-(μ-O)-Ca cubane motifs with Mn^{IV}–Ca distances of ~3.18 Å. A similar distance (3.15 Å) is also present in the marokite structure for one of the Mn–Ca distances of the Mn_3Ca cubanes present there. The plot was composed from 900 individual fits with shells from Table 1 plus one additional Mn–Mn shell at around 3 Å. The range for the calculation of the R_F-factor was 2 – 4 Å. Debye-Waller parameters for the two metal shells at around 3.14 Å were fixes to 0.054 Å. Other parameter were either varied freely (distances and coordination numbers) or fixed (Debye-Waller parameter) as indicated in Table 1.

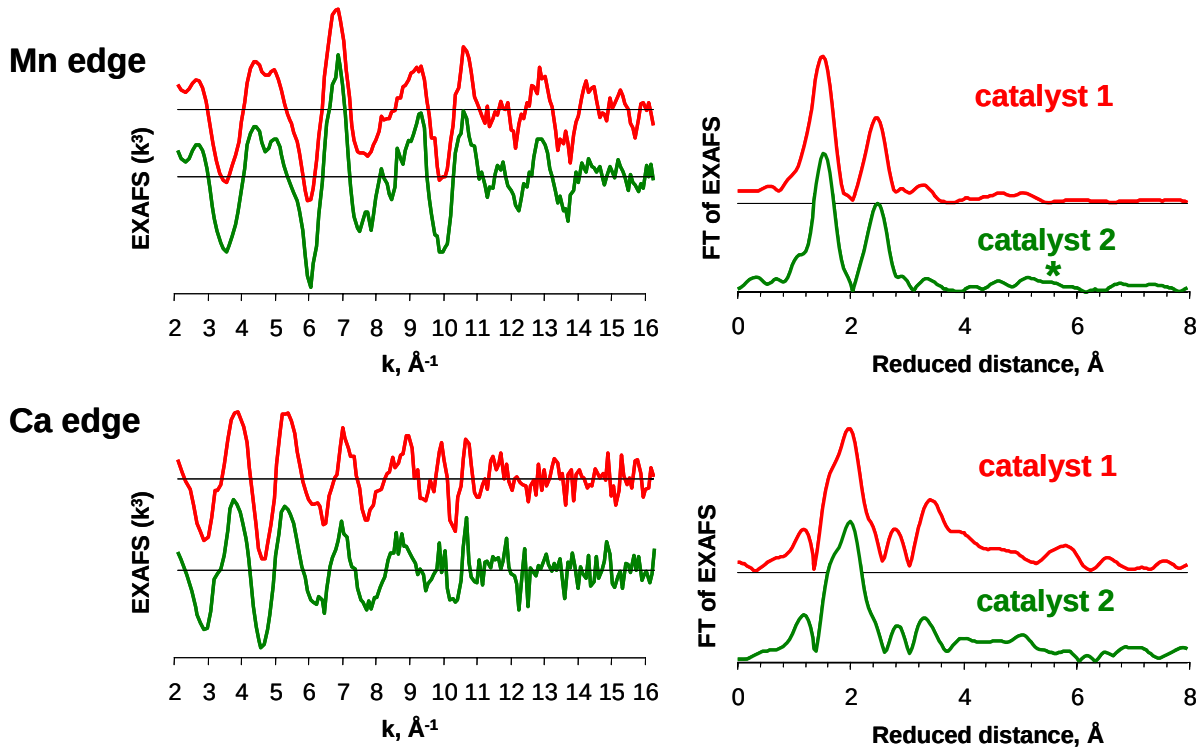

Figure S7. EXAFS spectra of oxide **1** (catalyst 1) and **2** (catalyst 2). The spectra and the corresponding Fourier transforms exhibit striking similarities. In catalyst **2,** there is a higher extent of long-range order. The asterisk (Fourier transform of the Mn EXAF) indicates a feature assignable to the doubled distance of 2.87 Å (= 5.74 Å), which is indicative for an extended structure of interconnected cubanes. For catalyst **1** an FT peak assignable to a distance of 5.74 Å is not detectable.

Table S1. Parameters for simulation of the EXAFS spectra of oxide **2**. For further details, see legend of Table 1 in the main manuscript.

Mn edge				Ca edge			
Shell	R (Å)	N	σ (Å)	Shell	R(Å)	N	σ (Å)
O^1	1.90 <0.01	5.4 -	0.063 0.019	O^1	2.38 0.01	7.4 -	0.109 0.037
O^1	2.28 0.04	0.6 0.2	0.063*	O^1	2.92 0.06	0.6 0.5	0.063*
Mn^2	2.87 <0.01	3.2 0.2	0.063*				
Ca^3	3.12 0.02	0.7 0.4	0.063*	Mn^2	3.16 0.03	0.4 0.2	0.063*
Ca^4	3.85 0.03	0.8 0.5	0.063*	Mn^3	3.76 0.02	0.7 0.3	0.063*
				Ca^4	4.10 0.08	0.3 0.5	0.063*
				Ca^4	4.40 0.05	0.6 0.6	0.063*
				Ca^4	4.73 0.05	0.8 0.7	0.063*
Mn^5	4.99 0.04	1.0 0.8	0.063*	Ca^5	5.05 0.05	0.9 0.9	0.063*
Mn^6	5.52 0.02	3.2 1.1	0.063*	Ca^6	5.31 0.04	1.5 1.1	0.067*
Mn^{MS}	5.74 -	1.1 0.5	0.063*				

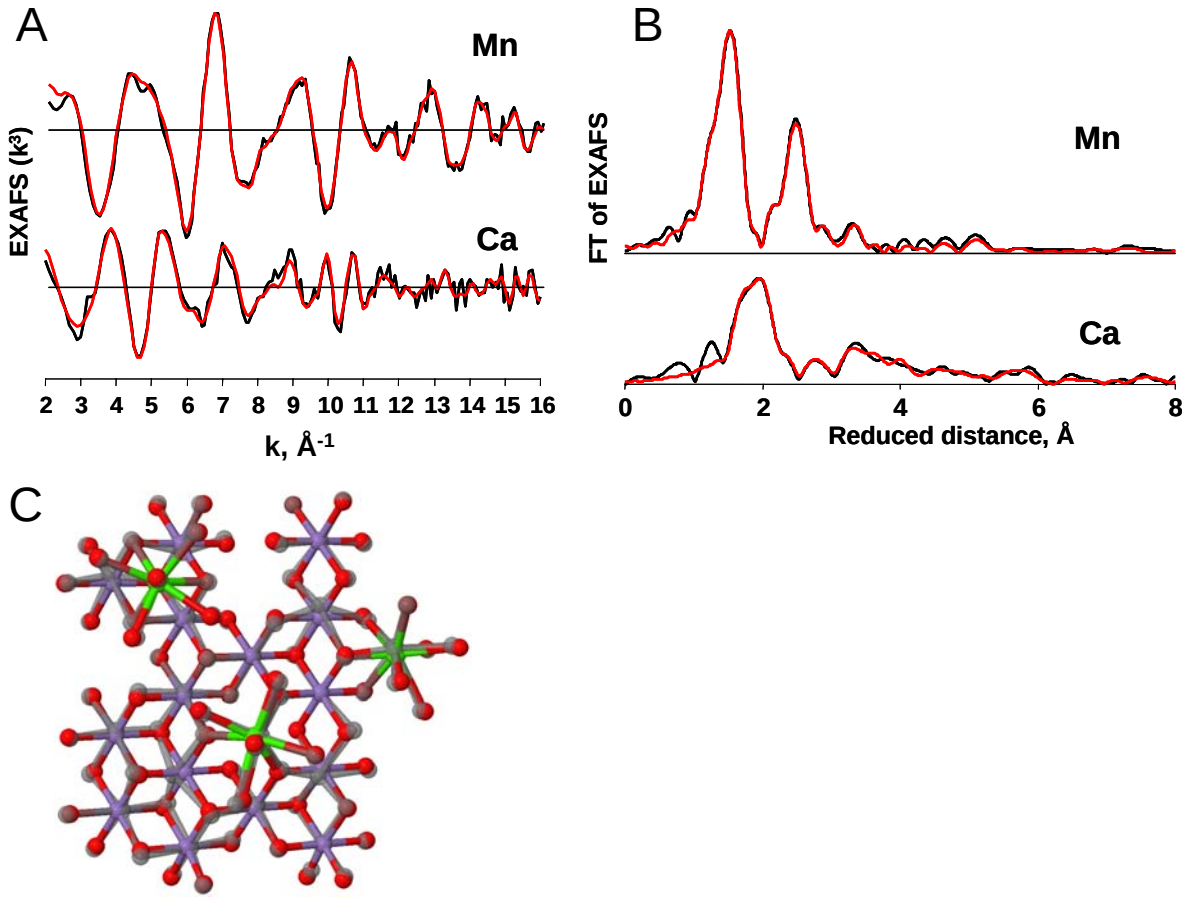

Figure S8. Top – Experimental (black) and simulated (red) EXAFS spectra of oxide **1**, for simulations involving the extended structural model shown in C. In A, spectra on a *k*-vector axis*;* in B, Fourier-transformed spectra. *Black lines* - experimental EXAFS spectra of **1** recorded at both the Mn and the Ca *K*-edge. *Red lines* - simulated EXAFS spectra based on the structural model presented in C. Each atom was considered as an individual backscatterer shell with a Debye-Waller parameter of 0.03 Å. *Bottom scheme* (in C) – initial structure and modified atom positions (the latter in grey).

References

1. C. D. Ling, J. J. Neumeier and D. N. Argyriou, *J. Solid State Chem.*, 2001, 160, 167-173.
2. A. Manceau, C. Tommaseo, S. Rihs, N. Geoffroy, D. Chateigner, M. Schlegel, D. Tisserand, M. A. Marcus, N. Tamura and Z.-S. Chen, *Geochim. Cosmochim. Acta*, 2005, 69, 4007-4034.
3. D. A. McKeown and J. E. Post, *Am. Mineral.*, 2001, 86, 701-713.
4. I. Saratovsky, P. G. Wightman, P. A. Pasten, J.-F. Gaillard and K. R. Poeppelmeier, *J. Am. Chem. Soc.*, 2006, 128, 11188-11198.
5. S. M. Webb, C. C. Feller, B. M. Tebo and J. R. Bargar, *Environ. Sci. Technol.*, 2006, 40, 771-777.
6. M. Zhu, M. Ginder-Vogel, S. J. Parikh, X.-H. Feng and D. L. Sparks, *Environ. Sci. Technol.*, 2010, 44, 4465-4471.
7. J. E. Post, *Proc. Natl. Acad. Sci. USA*, 1999, 96, 3447-3454.
8. S. Geller, *Acta Crystallogr., Sect. B: Struct. Sci.*, 1971, 27, 821-828.
9. A. L. Ankudinov, B. Ravel, J. J. Rehr and S. D. Conradson, *Phys. Rev. B*, 1998, 58, 7565-7576.
10. J. J. Rehr and R. C. Albers, *Rev. Mod. Phys.*, 2000, 72, 621-654.
11. W. H. Press, S. A. Teukolsky, W. T. Vetterling and B. P. Flannery, *Numerical Recipes in C: The Art of Scientific Computing, Second Edition*, Cambridge University Press, Cambridge, New York, Port Chester, Melbourne, Sydney, 1992.